

The Geometry of Mass Outflows and Fueling Flows in the Seyfert 2 Galaxy Mrk 3¹

D.M. Crenshaw², S.B. Kraemer³, H.R. Schmitt⁴, Y.L. Jaffé⁵, R.P. Deo⁶, N.R. Collins⁷, and T.C. Fischer²

ABSTRACT

We present a study of the resolved emission-line regions and an inner dust/gas disk in the Seyfert 2 galaxy Mrk 3, based on *Hubble Space Telescope* observations. We show that the extended narrow-line region (ENLR), spanning ~ 4 kpc, is defined by the intersection of the ionizing bicone of radiation from the AGN and the inner disk, which is not coplanar with the large-scale stellar disk. This intersection leads to different position and opening angles of the ENLR compared to the narrow-line region (NLR). A number of emission-line arcs in the ENLR appear to be continuations of dust lanes in the disk, supporting this geometry. The NLR, which consists of outflowing emission-line knots spanning the central ~ 650 pc, is in the shape of a backwards S. This shape may arise from rotation of the gas, or it may trace the original fueling flow close to the nucleus that was ionized after the AGN turned on.

Subject headings: galaxies: Seyfert – galaxies: individual (Mrk 3)

¹Based on observations made with the NASA/ESA Hubble Space Telescope, obtained at the Space Telescope Science Institute, which is operated by the Association of Universities for Research in Astronomy, Inc. under NASA contract NAS 5-26555.

²Department of Physics and Astronomy, Georgia State University, Astronomy Offices, One Park Place South SE, Suite 700, Atlanta, GA 30303; crenshaw@chara.gsu.edu

³Institute for Astrophysics and Computational Sciences, Department of Physics, The Catholic University of America, Washington, DC 20064

⁴Remote Sensing Division, Naval Research Laboratory, Washington, DC 20375; and Interferometrics, Inc., Herndon, VA 20171

⁵School of Physics and Astronomy, University of Nottingham, University Park, Nottingham NG7 2RD, UK

⁶Department of Physics, Drexel University, 3141 Chestnut St., Philadelphia, PA 19104

⁷Astrophysics Science Division, Code 667, Goddard Space Flight Center, Greenbelt, MD 20771

1. Introduction

Mrk 3 (UGC 3426) has been classified as an SB0 (Adams 1977) or S0 galaxy (Windhorst et al. 2002). It has been studied extensively in all wavebands, because it harbors a bright active galactic nucleus (AGN). It is a Seyfert 2 galaxy, because its optical spectra show only narrow ($\text{FWHM} < 1000 \text{ km s}^{-1}$) emission lines except in polarized-light spectra, which reveal broad emission lines from a Seyfert 1-like nucleus (Schmidt & Miller 1985; Miller & Goodrich 1990; Tran 1995). The central nucleus, which contains the supermassive black hole (SMBH), accretion disk, and broad-line region (BLR), is hidden from our direct line of sight by a large column ($N_H \approx 1.3 \times 10^{24} \text{ cm}^{-2}$) of cold dusty gas (Pounds & Page 2005; Bianchi et al. 2005), presumably in the shape of a torus (Antonucci 1993). At a redshift of $z = 0.013509$ based on H I 21-cm radiation (Tifft & Cocke 1988), Mrk 3 is at a distance of $\sim 55 \text{ Mpc}$ (for $H_0 = 73 \text{ km s}^{-1} \text{ Mpc}^{-1}$); at this distance, $1''$ corresponds to a transverse size of 270 pc .

Ground-based images of Mrk 3 in the B and I filters (Wagner 1987; Schmitt & Kinney 2000) show a host galaxy that is only slightly inclined, with an ellipticity $e = 0.16$ (inclination $i = 33^\circ$) and position angle $P.A. = 28^\circ$, based on its outer I-band isophotes at $r = 30'' - 40''$ from its nucleus. The ellipticity increases to $e = 0.36$ at $r = 10''$ at the same $P.A.$, suggesting the presence of a stellar bar and supporting an SB0 classification.

Hubble Space Telescope (*HST*) images of Mrk 3 in the light of [O III] at an angular resolution of $\sim 0''.1$ (Capetti et al. 1995, 1996, 1999; Schmitt & Kinney 1996; Schmitt et al. 2003) reveal that its narrow-line region (NLR) consists primarily of resolved emission-line knots extending over $\sim 2''.4$ ($\sim 650 \text{ pc}$), arranged in a backwards S configuration resembling a grand-design spiral, similar to that seen in several other Seyfert galaxies (Schmitt et al. 2003). High-resolution radio observations (Kukula et al. 1993; 1999) show radio knots along opposing jets that are nearly coincident with the linear portion of the NLR, but at slightly different position angles ($P.A. = 82^\circ$ for the jets, 71° for the NLR). The jets are slightly curved at their ends, in the direction of the offset emission-line knots that define the S-like structure of the NLR, as shown in Figure 1 (from Figure 4 in Kukula et al. 1999).

Outside of the NLR, emission-line images of Mrk 3 show an extended NLR (ENLR) with an overall shape that resembles a projected bicone, first noticed in ground-based observations (Pogge & DeRobertis 1993), extending over a range of $\sim 15''$ ($\sim 4 \text{ kpc}$). Many Seyfert galaxies show ENLRs, and their high ionization levels and often biconical shapes suggest they are ionized by the central AGN. Their relative faintness and distinct kinematics (dominated by rotation) compared to NLRs indicate that ENLRs arise from ionization of the gas in galactic disks by the AGN (Unger et al. 1987). The above *HST* studies revealed that the ENLR in Mrk 3 shows significant structure, which can be seen not only in the narrow-band emission-

line images but also in some of the broad-band images as well, such as in the WFPC2 F606W image (Malkan, Gorjian, & Tam 1998), due to inclusion of strong emission lines such as [O III] $\lambda\lambda 4959, 5007$ and $H\alpha$ in the bandpass. The F606W image also includes a strong contribution from the stellar continuum emission as well, which can be used to identify dust structures in the circumnuclear regions.

2. Previous Work and Open Questions

In Figure 2, we show a structure map¹ of the F606W image of Mrk 3 that highlights the small-scale structure of the emission-line regions and dust lanes, as well as the overall geometry of the NLR and ENLR. As noted by others (Wagner 1987; Haniff, Wilson, & Ward 1988; Capetti et al. 1995), the ENLR, defined by the faint emission-line arcs at greater distances from the nucleus than the S-shaped NLR, appears to be rotated and spans a narrower opening angle than the NLR (see also Figure 7). Thus, one question we would like to address in this paper is: why are the position angle and opening angle of the ENLR different from those of the NLR?

Figure 2 shows that much of the ionized gas in the ENLR of Mrk 3 is in the form of curved structures, such as arcs or pieces of spirals. Furthermore there appears to be a connection between some of these structures and the dust lanes to the NE, similar to that seen in the NLR of the Seyfert 2 galaxy Mrk 573 (Quillen et al. 1999; Pogge & Martini 2002; Martini et al. 2003a). Together, these features are similar in appearance to the nuclear dust spirals found in most Seyfert galaxies (Regan & Mulchaey 1999; Pogge & Martini 2002, Martini et al. 2003a), which likely trace the fueling flows to the AGN in the inner few kiloparsecs (Martini et al. 2003b; Deo et al. 2006; Simões Lopes et al. 2007). Another interesting question is therefore: what is the nature of the structure in the ENLR, and how is it related to the dust lanes that are outside of the ionizing bicone?

In Ruiz et al. (2001), we presented long-slit and slitless spectra of Mrk 3 obtained with the Space Telescope Imaging Spectrograph (STIS) on *HST*, which we used to study the kinematics of the emission-line knots in the NLR based on the [O III] $\lambda 5007$ emission line. We found that the spatially-resolved spectra could be matched with a biconical outflow

¹A structure map is the correction image obtained from the second iteration of a Richardson-Lucy reconstruction. Starting with an appropriate *HST* point-spread function (PSF), one divides the original image with a PSF-convolved version of the image and multiplies the resulting image with the transpose of the PSF. This procedure results in an image with the high-frequency component enhanced in contrast (Pogge & Martini 2002; Deo et al. 2006).

model that incorporates increasing velocity from near zero km s^{-1} at the nucleus (in the galaxy’s rest frame) to $\sim 800 \text{ km s}^{-1}$ (in the line of sight) at $0''.3$ from the nucleus, followed by decreasing velocity to near zero km s^{-1} at an angular distance of $\sim 1''.0$. Our model adopted a rather narrow bicone (maximum half-opening angle $[\theta_{max}] = 22.5^\circ$) with its axis positioned along the central linear structure in Figure 2 ($P.A. = 71^\circ$), corresponding to our slit location (see Ruiz et al. 2001). However, this bicone does not include the offset knots to the east and west that define the S shape. Thus, we would like to re-examine this problem and address a third question: what is the nature and origin of this shape, and can it be reconciled with our general picture of radial outflow?

In a previous paper (Collins et al. 2005), we modeled the geometry of the circumnuclear regions in Mrk 3. For the NLR bicone, we used the parameters from our kinematic models of the outflow (Ruiz et al. 2001), which are the $P.A.$ of the bicone axis, the inclination (i) of the bicone axis (zero is defined to be in the plane of the sky), and the half-opening angle of the outer edge of the bicone (θ_{max}). For the galactic disk we used the $P.A.$ and i from ground-based images of the galaxy (Schmitt & Kinney 1996). Based on the dust lanes seen in Figure 2, we suggested that the east side of the disk is closer to us.

There are several problems with the above interpretation as it relates to our open questions. First, the model cannot explain the observed ENLR. As can be seen in Collins et al. (2005, Figure 20), the intersection between the bicone and galactic disk defines the ENLR (seen clearly in the NE) which has an axis of symmetry at smaller $P.A.$ s than the NLR, the opposite of what is observed. If we make the west side of the disk closer to us, keeping the same values for the other parameters, the effect is the same, because the major axis of the disk lies roughly along the NE-SW edge of the bicone, and inclining the disk in either direction brings the E-W edge out of the disk. The second problem is that the dust lanes are approximately parallel to the minor axis of this disk, not the major axis as expected. Finally, the bicone as originally defined is rather narrow, and does not include the offset knots on either side of the inner, linear portion of the NLR or the ENLR, which lies in the same direction as the offset knots. Thus, we have undertaken a study to address these problems and the open questions that we have posed. First, we describe a new analysis of existing *HST* emission-line images to examine the ionization structure of the NLR in Mrk 3. Then, we re-examine the geometry of the NLR, ENLR, and dust structures in Mrk 3 in order to obtain a much better match to the observational constraints. Finally, we discuss how our geometric model provides new insights into the nature of fueling flows and outflows in this Seyfert galaxy.

3. Ionization Structure of the NLR and ENLR

We generated an ionization map of the circumnuclear regions in Mrk 3 by constructing an $[\text{O III}] \lambda 5007/[\text{O II}] \lambda 3737$ ratio image, to probe the geometry and structure of these regions. The observations were obtained with the post-COSTAR Faint Object Camera (FOC) on *HST* in the f/151, 512×512 mode, yielding a pixel size of $0''.014$ (the angular resolution is $\sim 0''.1$ FWHM). These observations were made as part of the project GO-5140 (P.I. Macchetto) on 1994 March 20. A log of the observations is presented in Table 1.

The images were retrieved from the *HST* archive, reduced, and calibrated using standard procedures (see Schmitt & Kinney 1996 for more details). The images were aligned, background subtracted using regions free of emission in the chip, and calibrated using information available in the header. The continuum image was used to subtract the host galaxy contribution to the emission-line images. This was done by scaling the flux of the continuum image based on the width of the two filters. We used the same continuum image for both on-line images. Although it would have been better to use a bluer continuum image for the subtraction of the host galaxy contribution to the $[\text{O II}]$ image, the only continuum image that was not strongly contaminated by line emission was that obtained with the F550M filter. This choice should not significantly affect the resulting continuum-subtracted $[\text{O II}]$ image. The host galaxy of Mrk 3 is an SBO, so we do not expect large color variations along the galaxy or large amounts of dust. We checked on whether this procedure over- or under-subtracted the host galaxy by inspecting the outer regions of the pure emission-line images, and further small corrections were applied when necessary to reduce the residuals. We estimate that the uncertainty in the continuum subtraction is on the order of 5%.

The final steps of the data reduction involved the determination of the noise in regions free from emission, used to determine the uncertainty in the flux measurements. Based on the $[\text{O II}]$ image, the one with the highest noise, we created a mask that blanked all regions with flux below the 3σ level. This mask was applied to both images, to ensure that we were not comparing regions with strong emission in one image with noise in the other. The blanked $[\text{O II}]$ and $[\text{O III}]$ images were used to measure the emission line fluxes in different regions of the NLR. This was done using 15 concentric circular annuli, 8 pixels ($\sim 0.1''$) wide. Each annulus was split into 20 sectors, with widths of 18° . Sectors with more than 50% of the $[\text{O II}]$ or $[\text{O III}]$ pixels blanked were eliminated from our analysis.

In Figure 3, we show the $[\text{O III}]/[\text{O II}]$ ratio image, and in Figure 4, we show plots of the $[\text{O III}]/[\text{O II}]$ ratio as function of *P.A.* at various distances from the central nucleus. Outside of the central nucleus, the ratio peaks at values of 4 – 6 around position angles $\sim 100^\circ$ and $\sim 240^\circ$, at the locations of bright emission-line knots across the NLR, consistent with the STIS long-slit values in Collins et al. (2005). These ratios hold for the eastern offset knot

and the core of the western offset knots, indicating ionization levels similar to those in the inner, linear portion of the NLR. The more diffuse emission surrounding the western knot and the northern edge of the NLR have somewhat lower values, indicating lower ionization parameters. These results are consistent with the suggestion by Collins et al. (2009) that there is lower ionization gas along the edges of the bicone that is due to filtering of the ionizing radiation by an absorber that is close to the central source. The [O III]/[O II] ratios in the ENLR (right-side plots in Figure 4) are lower, although still AGN-like, which could be due to filtering of the ionizing radiation as it traverses the ENLR disk.

The high ionization levels and high emissivities of the offset knots demonstrates that they see the ionizing flux directly and are therefore not “fossil nebulae”, in which the ionizing radiation has been cut off (Binette & Robinson 1987). Thus, the offset knots are in the ionizing bicone, which must be much wider than we previously assumed. Furthermore, the differences in $P.A.$ between the central NLR versus the offset knots and ENLR cannot be explained by a change in the $P.A.$ of a narrow bicone of ionizing radiation, due, for example, to precession of an optically-thick torus. The light-travel time to the ends of the linear portion of the NLR is ~ 1000 yr, which indicates that the bicone has maintained its current position for at least this long. If we assume that the jets are traveling at $\sim 0.1c$ (Ulvestad 2005, and references therein), the linear structure out to large distances indicates they have maintained their positions for even longer, $\sim 10,000$ yr. The recombination time for [O III] is $t_{rec} \approx [\alpha(O^{+2}, T) n_e]^{-1}$, where the recombination coefficient $\alpha(O^{+2}, T) = 1.72 \times 10^{-11} \text{ cm}^3 \text{ s}^{-1}$ at $T = 10,000\text{K}$ (Osterbrock & Ferland 2006). After ~ 1000 yr or longer, the O^{+2} in the offset knots and ENLR would have recombined, unless the electron densities are $n_e < 2 \text{ cm}^{-3}$. This is not feasible, because such low densities would lead to very low emissivities and the emission-line knots would not be visible. In fact, according to the trend of decreasing density from the nucleus from our studies of the STIS long-slit spectra of Mrk 3 (Collins et al. 2009), the offset knots should have a density of $n_e \approx 1000 \text{ cm}^{-3}$, yielding a recombination time of only ~ 2 yr for O^{+2} . Thus, precession is not a valid explanation for the different $P.A.s$ of the NLR and ENLR. Finally, if one supposed that the difference was due to gas in the ENLR rotating out of a narrow bicone, it would take $\sim 10^6$ yr, assuming a galactic rotational velocity of 250 km s^{-1} , so this is not a valid explanation either. Thus, we must look for another way to explain the different position and opening angles of the NLR and ENLR.

4. Modeling the Geometry of the NLR and ENLR

We have taken a fresh approach to the geometry of the NLR, inner disk, and ENLR. We remeasured the NLR bicone to include both the linear structure and offset knots, which

results in a much wider bicone at a somewhat larger $P.A.$, but with the same inclination angle. We take the apex of the bicone to be the location of the hidden nucleus established by ultraviolet imaging polarimetry (Kishimoto, et al. 2002), which is consistent with the location of the optical continuum peak and kinematic center of the NLR (Ruiz et al. 2001; Collins et al. 2005). We give our NLR bicone parameters, as well as our measurements of the projected ENLR, in Table 2. We determined an average $P.A.$ for the dust lanes of $129^\circ(\pm 6^\circ)$, and assumed this was the $P.A.$ of an inner dust/gas disk on the same scale as the ENLR. We again took the NE side of the disk to be the closer side, based on the presence of dust lanes only on this side. This is also consistent with our finding that the NLR emission is more reddened in the east than in the west (Collins et al. 2005). The only parameter that we did not determine directly was the inclination angle of the inner disk.

We have developed a geometric modeling program, similar to that used by Mulchaey et al. (1996), to visualize the intersection between the inner dust/gas disk and the bicone of ionizing radiation. We varied the inclination angle of the disk, which changes the intersection between the disk and bicone of ionizing radiation, to match the $P.A.$ and θ_{max} of the ENLR. We were able to match the measured values to within the measurement uncertainties ($\pm 2^\circ$) with $i = 64^\circ \pm 2^\circ$. Figure 5 shows the resulting geometric model from our viewpoint, and Figure 6 displays a view down the eastern cone. In Figure 5, the solid portion on the eastern side lies directly above the intersection between the eastern cone and disk – the ENLR is an extension of this triangle plus a symmetric triangle in the other direction, as shown in Figure 7. As shown in Figure 6, the intersection between the bicone and disk is in the southern part of the east cone, resulting in the smaller opening angle and shifted $P.A.$ of the ENLR compared to the NLR bicone as seen from the Earth.

Figure 7 shows the structure map from Figure 2, with the outlines of our geometric model superimposed. The model encompasses nearly all of the emission-line structure in both the NLR and ENLR, except for faint extensions of a couple of arcs in the ENLR. These can be explained by evidence in this paper and in Collins et al. (2009) that the bicone is not sharp-edged in Mrk 3, and this gas may in fact be ionized by weak, filtered radiation from the AGN at polar angles slightly greater than θ_{max} .

5. Conclusions

We have developed a new geometric model for the NLR and ENLR in the Seyfert 2 galaxy Mrk 3 that eliminates the discrepancies that we have encountered with our previous model (Ruiz et al. 2001; Collins et al. 2005), explains a number of observed properties of these regions, and helps to elucidate the geometry and nature of the fueling flows traced by

dust structures and outflows traced by ionized gas kinematics in the circumnuclear regions. Our new model has a much larger opening angle and a slightly different $P.A.$ for the radiation bicone, to explain the ionization of not only the inner, linear portion of the NLR, but the offset emission-line knots and the entire ENLR as well. We previously assumed an inner dust/gas disk that was at the same $P.A.$ and i as the disk of the host galaxy, but that lead to two problems: 1) the dust lanes are parallel to the minor axis of the disk, and 2) the intersection between the disk and radiation bicone cannot explain the differences between the NLR and ENLR in $P.A.$ and opening angle. However, by adopting an inner dust/gas disk that is parallel to the observed inner dust lanes and varying the inclination of the disk, we were able to match the geometry of the NLR and ENLR and explain these differences, answering our first open question.

Evidence for an inner dust/gas disk in Mrk 3 comes not only from the dust lanes to the NE of the nucleus, but from the emission-line arcs in the ENLR as well. In fact, it appears that in some cases, the emission-line arcs are continuations of the dust lanes into the ENLR, with the associated gas ionized by the AGN, supporting our claim that the geometry of the ENLR is due to the intersection between the dust/gas disk and the radiation bicone defined by the NLR, answering our second open question. This is the same scheme that has been proposed for the emission-line arcs in Mrk 573 (Quillen et al. 1999; Martini et al. 2003a; Schlesinger et al. 2009).

Where does the inner dust/gas disk come from? Noordermeer et al. (2005) discovered a bridge of H I emission between Mrk 3 and UGC 3422, a companion spiral galaxy ~ 100 kpc to the NW. They suggest that this gas, which shows a local concentration in Mrk 3, was tidally drawn out of the gas disk in UGC 3422. The bridge of gas is in the same general direction as the major axis of the inner disk in Mrk 3, which is at a $P.A. = 129^\circ$ (or -51°). This gas is therefore the likely source of the inner disk and the large-scale fueling flow to the AGN.

6. Discussion

We have shown how our new geometric model of Mrk 3 explains the different $P.A.s$ and opening angles of its NLR and ENLR, as well as the arc-like structure of the emission-line gas in the ENLR. The remaining question to be addressed is the nature of the backwards S shape of the NLR. This structure is not unique to Mrk 3, and may therefore be of some fundamental importance. From a study of the NLRs in 60 Seyfert galaxies using *HST* [O III] emission-line images (Schmitt et al. 2003), three others show well-defined S (or Z) shapes: NGC 3393 (Seyfert 2), NGC 3516 (Seyfert 1), and NGC 6860 (Seyfert 1). Several other

NLRs show curved structures or arcs, like those in Mrk 573 or in the ENLR of Mrk 3.

The offset knots that define the backwards S shape in Mrk 3 appear to be well separated from the inner, linear portion of the NLR, and lie along the same general direction as the ENLR. Thus, they could lie in the same disk as the ENLR, but their other properties are more like the NLR knots. They have higher emissivities and higher velocity dispersions than the ENLR knots (Ruiz et al. 2001), and their [O III]/[O II] ratios are similar to the other NLR knots; these all suggest that they belong to the NLR. Because the offset knots lie in the same direction as the ENLR, they could possibly be located in the inner dust/gas disk. However, it is not clear where the linear portion of the NLR is located within the bicone. According to our geometry, the linear portion cannot be in the inner disk, unless the disk begins to warp inside of the offset knots.

The kinematics of the NLR in Mrk 3 (Ruiz et al. 2001) follow the same pattern seen in the other three Seyfert galaxies that we have studied in detail using STIS long-slit spectra: NGC 4151 (Das et al. 2005), NGC 1068 (Das et al. 2006), and Mrk 573 (T. Fischer, et al., in preparation). The emission-line knots have their own peculiar velocities superimposed on a general pattern of radial outflow. So how does the backwards S shape of the NLR in Mrk 3 fit into our picture of radial outflow? If all of the outflowing gas in the NLR came from close to the nucleus (e.g., inside of ~ 30 pc, a resolution element), then how did this shape come about? It could result from rotation of the outflowing gas, due to its initial angular momentum, or it could come from collision of the gas with the rotating inner disk. An advantage of the latter is that it might explain the curved ends of the radio jets (Kukula et al. 1993). Unfortunately, we cannot test for rotation, because we only have one STIS long-slit observation, which does not pass through the offset NLR knots. The STIS slitless data are much less precise; they indicate that the eastern offset knot is blueshifted by ~ 250 km $^{-1}$ and the western offset knot is blueshifted by ~ 50 km $^{-1}$ (Ruiz et al. 2001), but the latter is uncertain by at least 50 km s $^{-1}$ due to the diffuseness of this knot. STIS long-slit spectra of the offset knots, preferably at high spectral resolution, would be extremely useful for testing the rotation hypothesis.

Another possible explanation for the backwards S shape is that it was already present when the AGN turned on, after which at least some of the gas was ionized. One intriguing possibility is that this shape traces the original fueling flow to the nucleus on the scale of the NLR. This suggestion is motivated by the fact that this shape resembles a “grand-design” nuclear dust spiral, which has been seen on the same scale as the NLR in other Seyfert galaxies, along with other types of dust spirals (Martini et al. 2003a), and offers an efficient way to fuel the inner nucleus (Deo et al. 2006). This explanation is not inconsistent with radial outflow, since the time required to disrupt the S shape is rather long, on the order of

the NLR crossing time, which is $\sim 5 \times 10^5$ yr for a distance of 300 pc and a typical NLR cloud velocity of 500 km s^{-1} .

The above explanation would imply that much of the outflow that we see in the NLR is due to in situ acceleration, rather than acceleration of clouds from close to the nucleus. Support for in situ acceleration comes from our determination that mass outflow occurs throughout the NLR in Mrk 3, and that the mass of the NLR is $\sim 1 \times 10^7 M_{\odot}$ (Collins et al. 2009). It seems unlikely that such a large amount of gas could originate from inside of the unresolved nucleus, with a transverse size ≤ 27 pc. Furthermore, we found that the mass outflow rate in the NLR is $\sim 15 M_{\odot} \text{ yr}^{-1}$, compared to the accretion rate of only $0.35 M_{\odot} \text{ yr}^{-1}$ needed to sustain its bolometric luminosity (Collins et al. 2009), and it is difficult to understand how all of this outflow could come from close in. However, in situ acceleration presents a couple puzzles. First, how does in situ acceleration explain the overall flow pattern in the NLR, in which velocity increases and then decreases with distance from the central AGN (Ruiz et al. 2001)? Second, why do the NLR clouds have low dust/gas ratios and relatively low optical depths (Collins et al. 2009), if they are accelerated off the cool inflowing gas?

A possible explanation is that the clouds are lifted off the fueling flow by a highly ionized wind, perhaps in the form of a thermal or Parker wind (Parker 1965). As suggested by Everett & Murray (2007), the velocities of the clouds are therefore controlled by the flow pattern of the wind. If the wind originates inside the dust sublimation radius, then it will be dust free, and mixing with the cooler gas in the clouds would lead to lower dust/gas ratios. Alternatively, the low dust/gas ratios could result from grain destruction during the interaction between the wind and the clouds. The wind modeled by Everett & Murray is more highly ionized than the X-ray emission line gas that is extended along the optical NLR in Mrk 3 (Sako et al. 2000; Bianchi et al. 2006), and it may have characteristics more in common with the material that scatters the hidden BLR emission into our line of sight. The major problem with this model is that the thermal wind likely accelerates too rapidly to account for the radial velocity profile observed in Seyfert NLRs (Everett & Murray 2007). Furthermore, it is unclear how a highly ionized wind could entrain the clouds, when the outward pressure, due to radiation, on the latter could be much greater than that on the wind. An alternative possibility is that the clouds are radiatively driven, but their acceleration is inefficient due to their interaction with the highly-ionized gas. The interaction is likely to produce Kelvin-Helmholtz instabilities, which may cause microturbulence (Kraemer, Bottorff, & Crenshaw 2007), resulting in the large observed velocity dispersions (Ruiz et al. 2005).

In any case, it is clear that the shapes of the NLR and ENLR in Mrk 3 are defined by the intersection of the ionizing bicone of radiation and the location of the gas. If the fueling

flow to the AGN is continuous and has not been disrupted by the outflow, the inner dust/gas disk must eventually warp to $P.A. \approx 0^\circ$ and $i = 5^\circ$ to form the putative optically-thick torus that produces the bicone of ionizing radiation in the Mrk 3. Observations of cold molecular gas at high angular resolution would help to identify possible warping and further elucidate the interaction between fueling flows and outflows in Mrk 3.

Some of the data presented in this paper were obtained from the Multimission Archive at the Space Telescope Science Institute (MAST). Support for this work was provided by NASA through grant number HST-AR-11243.04-A from the Space Telescope Science Institute, which is operated by AURA, Inc., under NASA contract NAS 5-26555.

Table 1. FOC Observing Log

Dataset Name	Exp. Time (s)	Filter	Comment
X2580103T	750	F502M	[O III] λ 5007
X2580104T	1196	F550M	Continuum
X2580102T	896	F372M	[O II] λ 3727

Table 2. Geometric Parameters for Mrk 3^a

Parameter	Old Values ^b	New Values ^b
<i>P.A.</i> (Disk)	28°	129°
<i>i</i> (Disk)	33°(NE)	64°(NE)
<i>P.A.</i> (NLR Bicone)	71°	89°
<i>i</i> (NLR Bicone)	5°(NE)	5°(NE)
θ_{max} (NLR Bicone)	25°	51°
<i>P.A.</i> (ENLR)	—	112°
θ_{max} (ENLR)	—	28°

^aThe letters in parentheses indicates the side closest to us.

^bOld values are for the outer stellar disk. New values are for the inner dust/gas disk.

REFERENCES

- Adams, T.E. 1977, *ApJS*, 33, 19
- Antonucci, R. 1993, *ARA&A*, 31, 473
- Bianchi, S., Miniutti, G., Fabian, A.C., & Iwasawa, K. 2005, *MNRAS*, 360, 380
- Bianchi, S., Guainazzi, M., & Chiaberge, M. 2006, *A&A*, 448, 511
- Binette, L. & Robinson, A. 1987 *A&A*, 177, 11
- Capetti, A., Axon, D.J., Macchetto, F.D., Sparks, W.B., & Boksenberg, A. 1996, *ApJ*, 469, 554
- Capetti, A., Axon, D.J., Macchetto, F.D., Marconi, A., & Winge, C. 1999, *ApJ*, 516, 187
- Capetti, A., Macchetto, F., Axon, D.J., Sparks, W.B., & Boksenberg, A. 1995, *ApJ*, 448, 600
- Collins, N.R., Kraemer, S.B., Crenshaw, D.M., Bruhweiler, F.C., & Melendez, M. 2009, *ApJ*, 694, 765
- Collins, N.R., Kraemer, S.B., Crenshaw, D.M., Ruiz, J., Deo, R., & Bruhweiler, F.C. 2005, *ApJ*, 619, 116
- Das, V., Crenshaw, D.M., Hutchings, J.B., Deo, R.P., Kraemer, S.B., Gull, T.R., Kaiser, M.E., Nelson, C.H., & Weistrop, D. 2005, *AJ*, 130, 945.
- Das, V., Crenshaw, D.M., Kraemer, S.B., & Deo, R.P. 2006, *AJ*, 132, 620
- Deo, R.P., Crenshaw, D.M., & Kraemer, S.B. 2006, *AJ*, 132, 321
- Everett, J.E. & Murray, N. 2007, *ApJ*, 656, 93
- Haniff, C.A., Wilson, A.S., & Ward, M.J. 1988, *ApJ*, 334, 104
- Kishimoto, M., Kay, L.E., Antonucci, R., Hurt, T.W., Cohen, R.D., & Krolik, J.H. 2002, *ApJ*, 567, 790
- Kraemer, S.B., Bottorff, M.C., & Crenshaw, D.M. 2007, *ApJ*, 668, 730
- Kraemer, S.B., Schmitt, H.R., & Crenshaw, D.M. 2008, *ApJ*, 679, 1128
- Kukula, M.J., Dunlop, J.S., McLure, R.J., Baum, S. A., O’Dea, C.P., & Hughes, D.H. 1999, *ApJ*, 518, 117
- Kukula, M.J., Ghosh, T., Pedlar, A., Schilizzi, R.T., Miley, G.K., de Bruyn, A.G., & Saikia, D.J. 1993, *MNRAS*, 264, 893
- Malkan, M.A., Gorjian, V., & Tam, R. 1998, *ApJS*, 117, 25
- Martini, P., Regan, M.W., Mulchaey, J.S., & Pogge, R.W., 2003a, *ApJS*, 146, 353

- Martini, P., Regan, M.W., Mulchaey, J.S., & Pogge, R.W., 2003b, *ApJ*, 589, 774
- Miller, J.S. & Goodrich, R.W. 1990, *ApJ*, 355, 456
- Mulchaey, J.S., Wilson, A.S., & Tsvetanov, A. 1996, *ApJ*, 467, 197
- Noordermeer, E., van der Hulst, J.M., Sancisi, R., Swaters, R.A., & van Albada, T.S. 2005, *A&A*, 442, 137
- Osterbrock, D.E. & Ferland, G.J. 2006, *Astrophysics of Gaseous Nebulae and Active Galactic Nuclei*, 2nd ed. (Sausalito, CA: Univ. Science Books)
- Parker, E.N. 1965, *SSrv*, 4, 666
- Pogge, R.W. & De Robertis, M.M. 1993, *ApJ*, 404, 563
- Pogge, R.W. & Martini, P. 2002, *ApJ*, 569, 624
- Pounds, K.A. & Page, K.L. 2005, *MNRAS*, 360, 1123
- Quillen, A.C., Alonso-Herrero, A., Rieke, M.J., McDonald, C., Falcke, H., & Rieke, G.H. 1999, *ApJ*, 525, 685
- Regan, M.W. & Mulchaey, J.S. 1999, *AJ*, 116, 2676
- Ruiz, J.R., Crenshaw, D.M., Kraemer, S.B., Bower, G.A., Gull, T.R., Hutchings, J.B., Kaiser, M.E., & Weistrop, D. 2001, *AJ*, 122, 2961
- Sako, M., Kahn, S.M., Paerels, F., & Liedahl, D.A. 2000, *ApJ*, 543, L115
- Schmidt, G.D. & Miller, J.S. 1985, *ApJ*, 290, 517
- Schmitt, H.R., Donley, J.L., Antonucci, R.R.J., Hutchings, J.B., & Kinney, A.L. 2003, *ApJS*, 148, 327
- Schmitt, H.R. & Kinney, A.L. 1996, *ApJ*, 463, 498
- Schmitt, H.R. & Kinney, A.L. 2000, *ApJS*, 128, 479
- Schlesinger, K., Pogge, R.W., Martini, P., Shields, J.C., & Fields, D. 2009, *ApJ*, 699, 857
- Simões Lopes, R.D., Storchi-Bergmann, T., de Fátima Saraiva, M., & Martini, P. 2007, *ApJ*, 655, 718
- Tift, W.G. & Cocke, W.J. 1988, *ApJS*, 67, 1
- Tran, H.D. 1995, *ApJ*, 440, 565
- Ulvestad, J.S. Wong, D.S., Taylor, G.B., Gallimore, J.F., & Mundell, C.G. 2005, *AJ*, 130, 936
- Unger, S.W., Pedlar, A., Axon, D.J., Whittle, M., Meurs, E.J.A., & Ward, M.J. 1987, *MNRAS*, 228, 671

Wagner, S.J. 1987, *A&A*, 185, 77

Windhorst, R.A., et al. 2002, *ApJS*, 143, 113

Fig. 1.— [O III] image (greyscale) of the NLR in Mrk 3 from the *HST* Faint Object Camera, with radio 18 cm emission (contours) superimposed, from Kukula et al. (1999, reproduced by permission of the authors and the AAS). Tick marks on the vertical axis are separated by $\sim 0''.2$. North is up and east is to the left for this image and all others.

Fig. 2.— Structure map of the *HST* WFPC2 image of Mrk 3 obtained with the F606W filter. The image is $23'' \times 23''$. Dark areas correspond to line emission and bright areas correspond to dust absorption. The white areas around the NLR are artifacts of the structure-map procedure.

Fig. 3.— [O III]/[O II] ratio map for the NLR in Mrk 3, based on *HST* images. The color bar below the image gives the range of [O III]/[O II] values.

Fig. 4.— [O III]/[O II] ratio as function of $P.A.$ at various distances from the central nucleus. Values for the NLR and ENLR are shown in the left and right plots, respectively.

Fig. 5.— Geometric model of the NLR bicone and inner disk in Mrk 3, based on the “new” parameters in Table 2. This figure shows the view from Earth. The NLR bicone axis is nearly in the plane of the sky (the eastern axis lies 5° out of the plane). The NE side of the disk is closer than the SW side and lies in front of most of the eastern cone.

Fig. 6.— Geometric model of the NLR bicone and inner disk in Mrk 3, based on the “new” parameters in Table 2. This figure shows a view down the eastern cone, with the view from Earth coming from the right, east almost directly out of the page, and north at the top.

Fig. 7.— Structure map of Mrk 3 with our model superimposed. We show the inner bicone of ionizing radiation, which encompasses the backwards S shape of the NLR. The outer triangular regions show the intersection between the bicone of ionizing radiation and the inner dusty disk, which encompasses the ENLR.

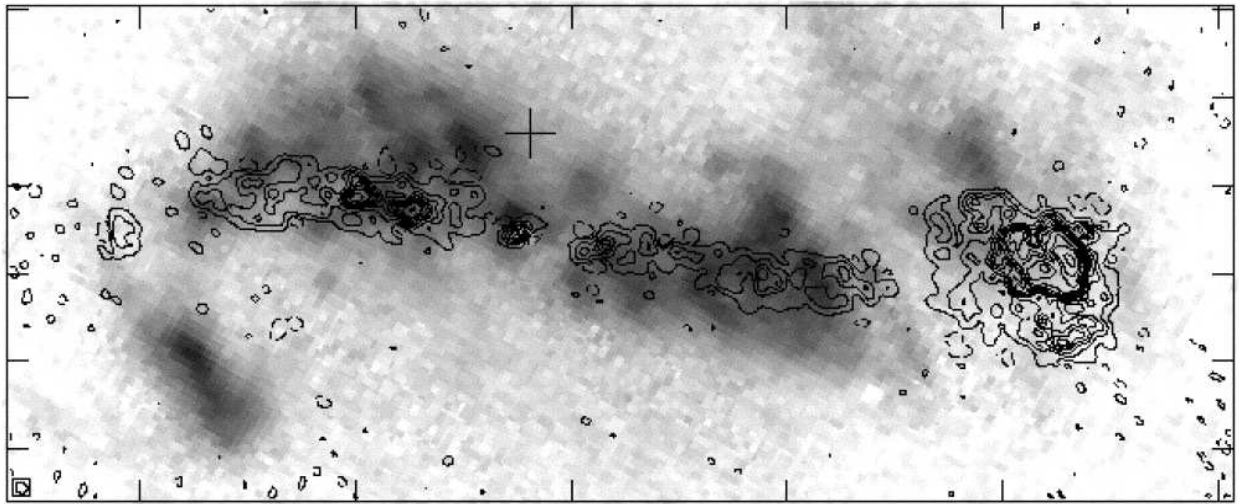


Fig. 1.

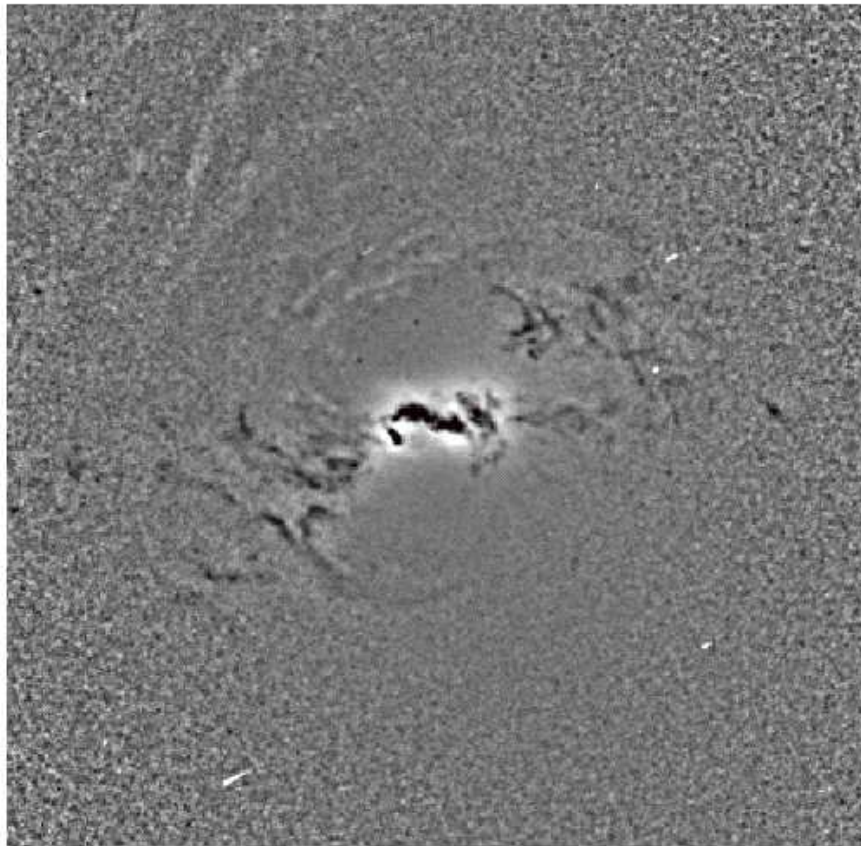


Fig. 2.

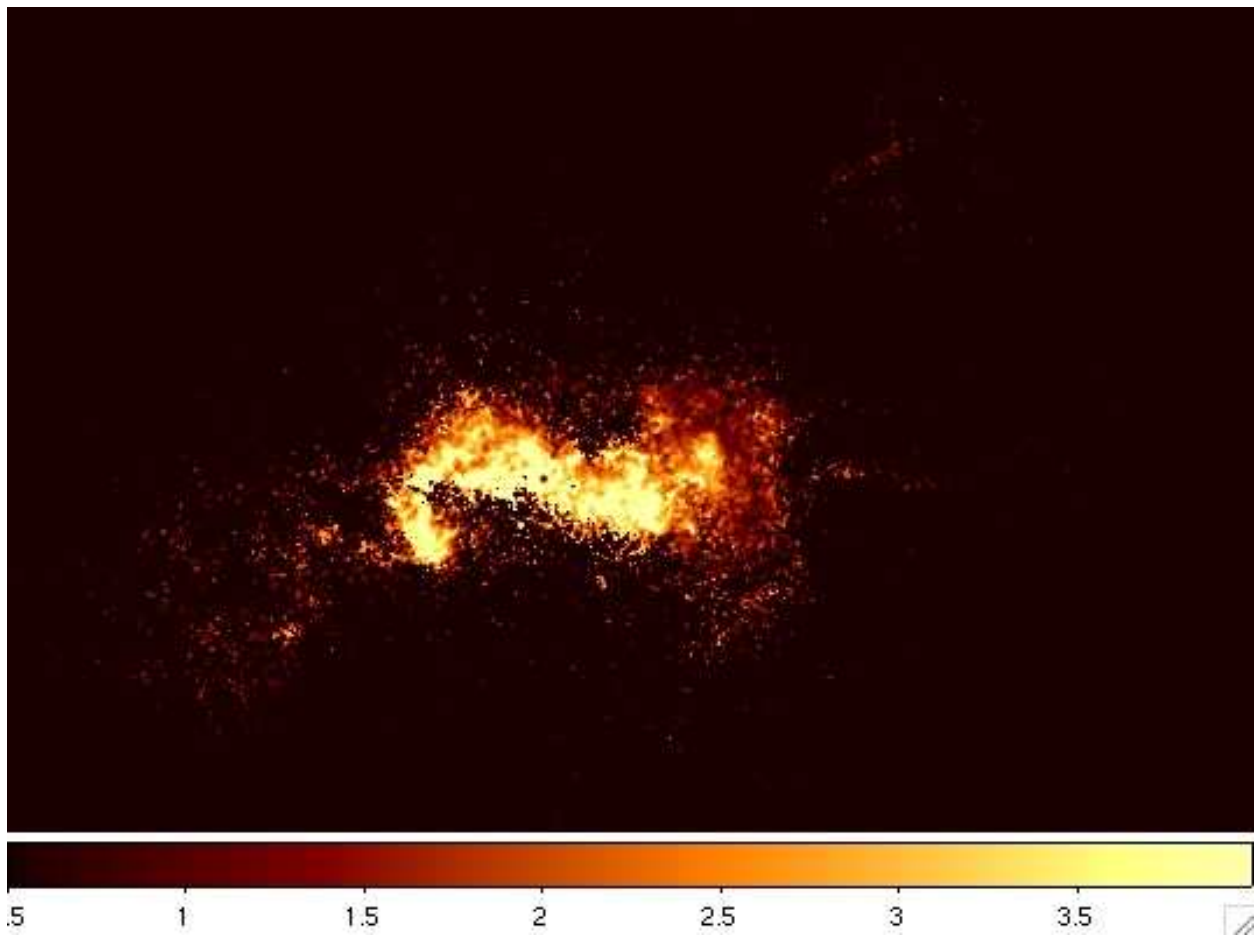


Fig. 3.

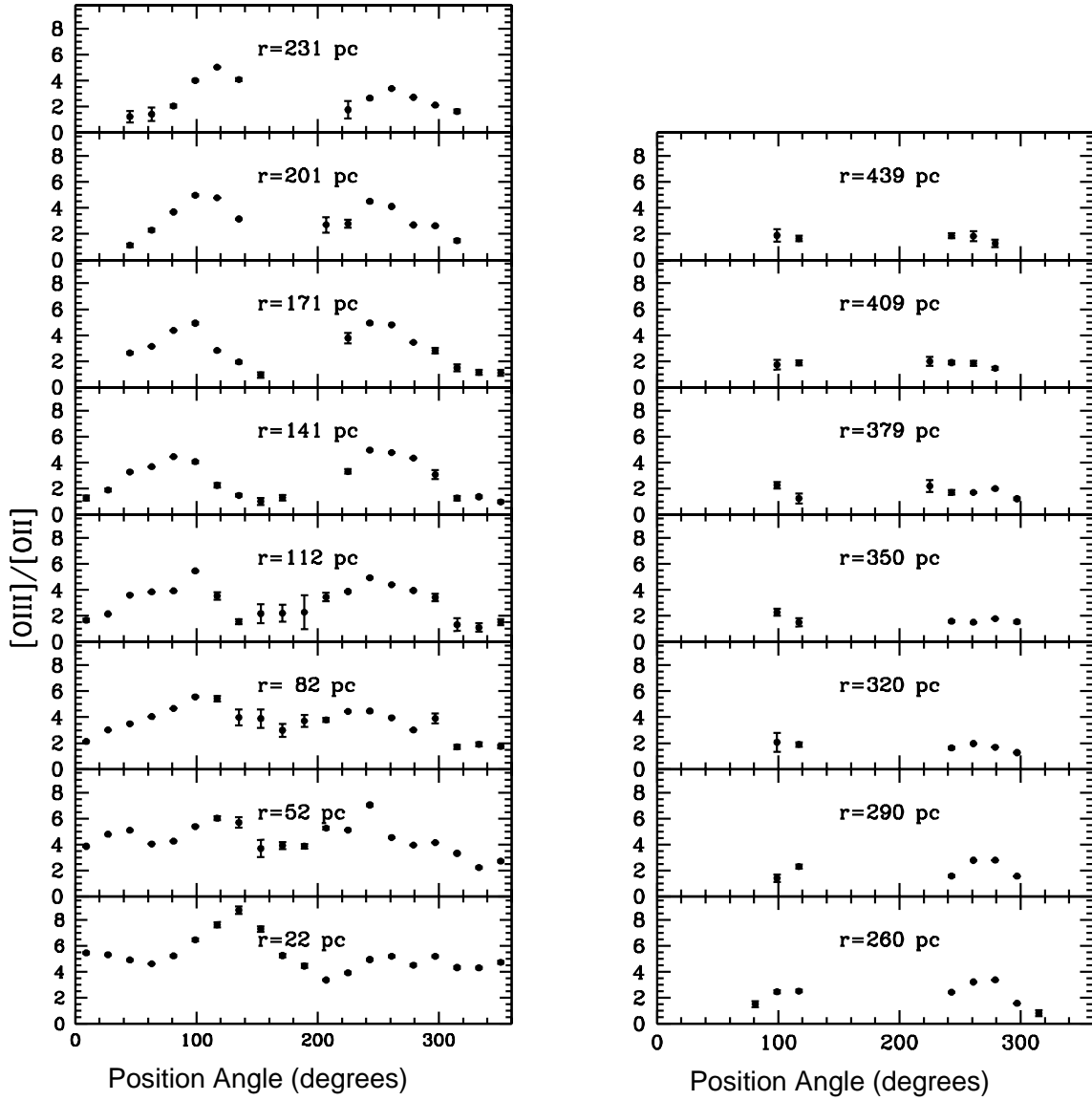


Fig. 4.

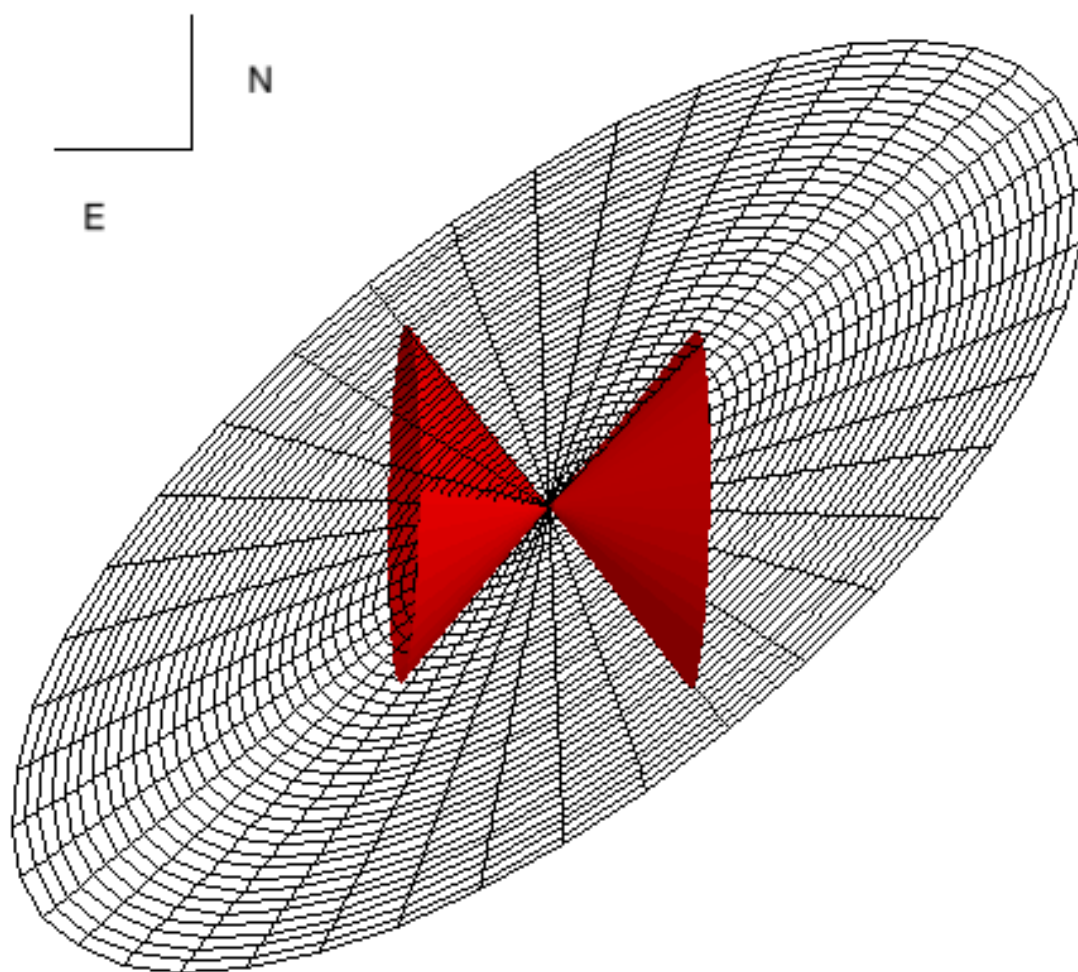


Fig. 5.

N - top of page
E - out of page

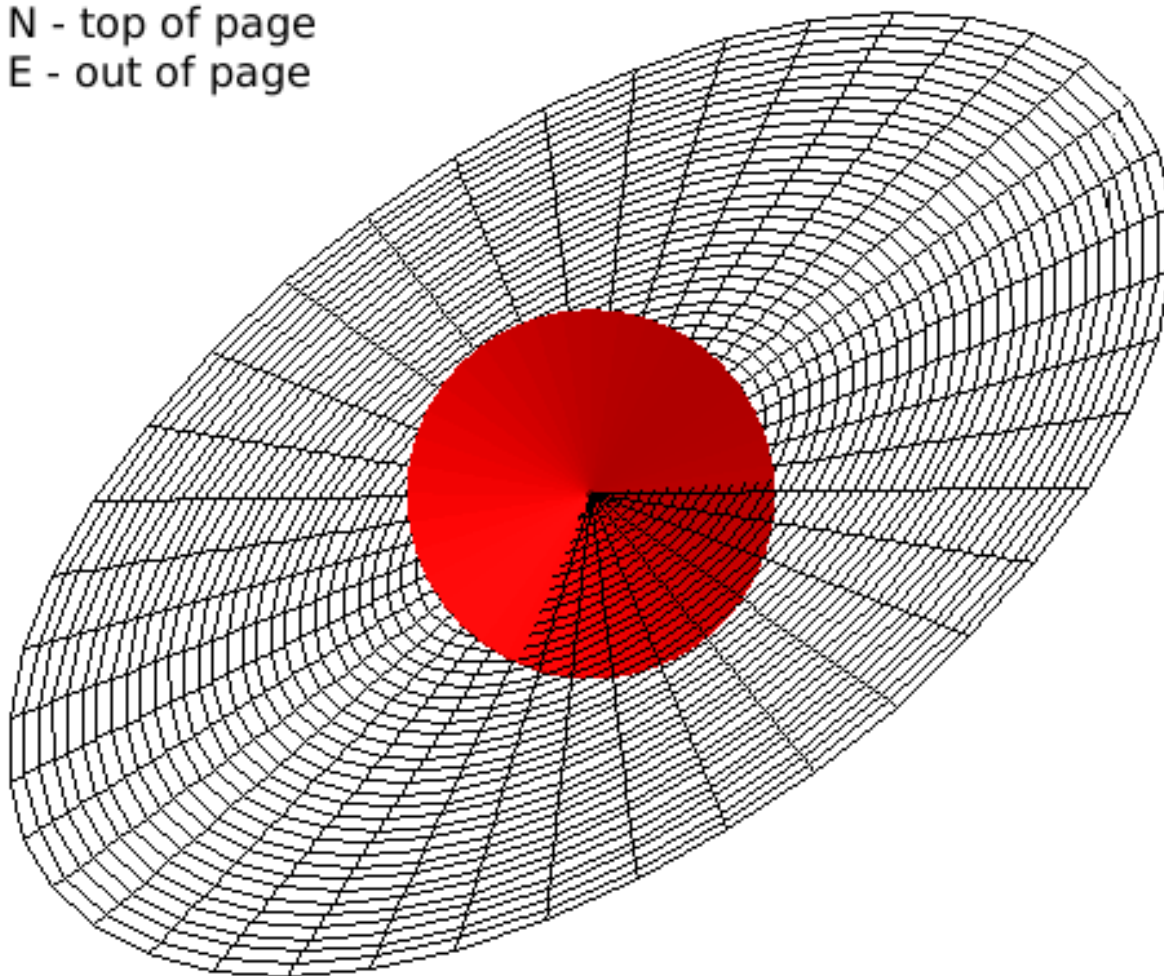


Fig. 6.

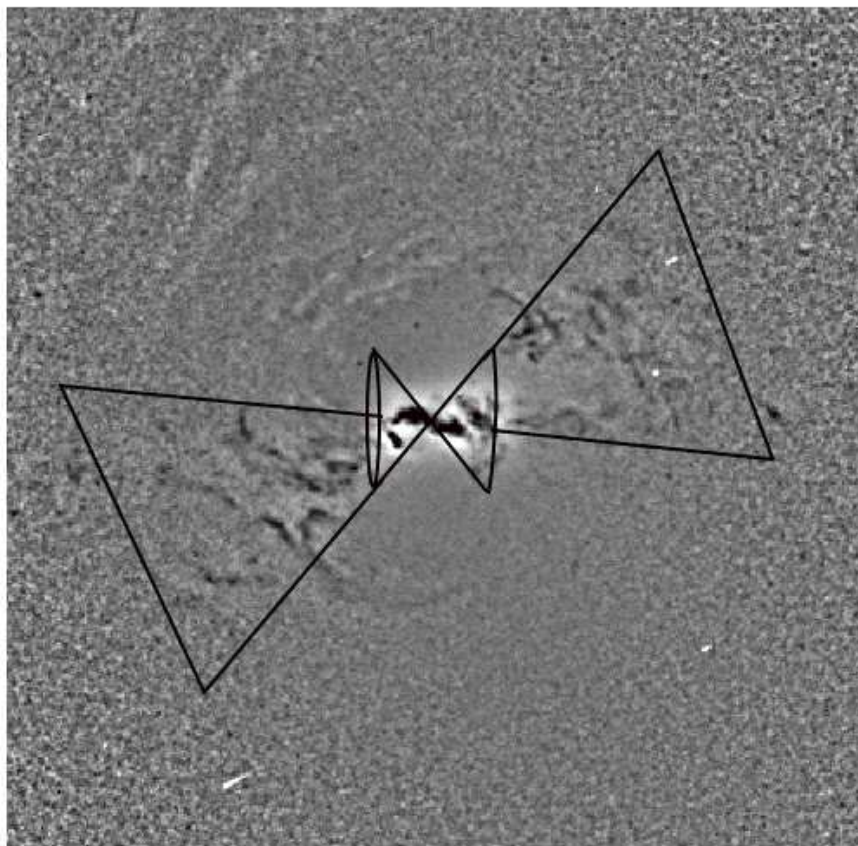


Fig. 7.